Opto-Electronic Advances

Supplementary information

November 2023, Vol. 6, No. 11

DOI: 10.29026/oea.2023.230094

Ferroelectrically modulate the Fermi level of graphene oxide to enhance SERS response

Mingrui Shao[1], Chang Ji[1], Jibing Tan[1], Baoqiang Du[1], Xiaofei Zhao[1], Jing Yu[1], Baoyuan Man[1], Kaichen Xu[2]*, Chao Zhang[1]* and Zhen Li[1]*

[1]Institute of Materials and Clean Energy, School of Physics and Electronics, Shandong Normal University, Jinan 250014, China; [2]State Key Laboratory of Fluid Power and Mechatronic Systems, School of Mechanical Engineering, Zhejiang University, Hangzhou 310030, China.
*Correspondence: KC Xu, E-mail: xukc@zju.edu.cn; C Zhang, E-mail: czsdnu@126.com; Z Li, E-mail: lizhen19910528@163.com

This file includes:

Supplementary information for this paper is available at https://doi.org/10.29026/oea.2023.230094

Section 1 Electrical properties of pyroelectric PMN-PT

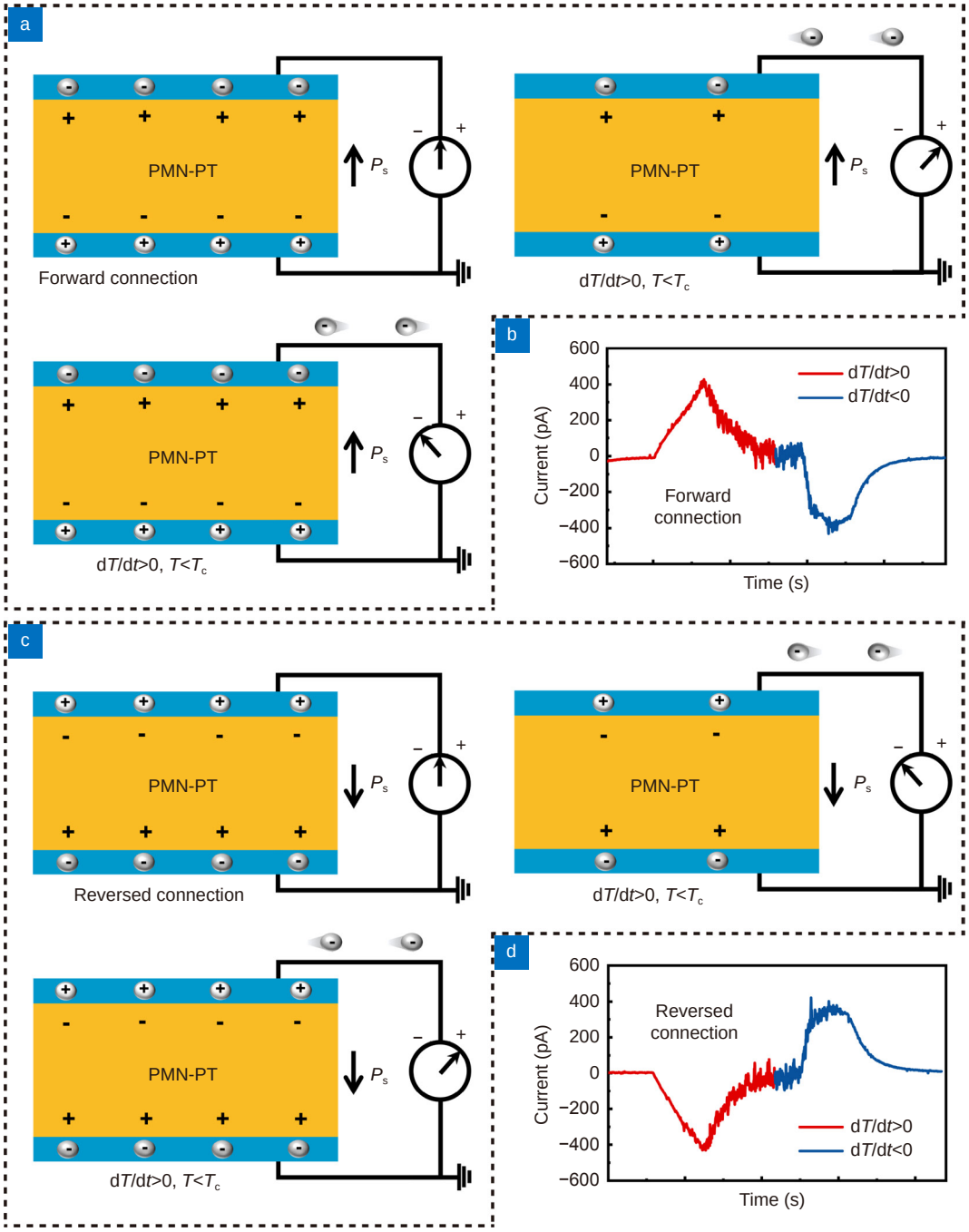

Fig. S1 | (**a**, **c**) Schematic diagram and (**b**, **d**) measured short-circuit current of pyroelectric PMN-PT at (a, b) forward connection and (c, d) reversed connection to the measurement system when the temperature changes from 20 to 100 °C (dT/dt > 0) and 100 to 20 °C (dT/dt < 0).

Before performing the short-circuit current test, both sides of the ferroelectric PMN-PT were coated with a thin silver film as electrodes using a vacuum thermal vaporizer (VZZ-300S, Beijing, China) with a deposition thickness of 10 nm and a deposition rate of 0.2 Å/s. SPI silver conductive paint (purchased from Wuhan Vacuum Tesco Trading Co., Ltd.) was used to fix two gold wires (the length of 10 cm; the diameter of 0.1 mm) to the surface of the upper and lower silver electrodes, respectively. The gold wires were then connected to a three-electrode electrochemical workstation (CH Instruments Ins., CHI760E). The working electrode (green) was linked to the upper silver electrode; the counter electrode (red) was linked to the lower silver electrode together with the auxiliary electrode (white), as shown in Fig. S1(a). Sub-

sequently, the Ag/PMN-PT/Ag sample was placed on a temperature console (LINKAM THMS600) to provide the temperature fluctuations. As the temperature of the sample increases from 20 to 100 °C ($dT/dt > 0$), a positive current is detected (Fig. S1(b)), indicating that the current flows from the counter electrode to the workstation (electrons flow from the working electrode to the workstation). The amplitude of the vibration of the electric dipole inside the PMN-PT along the central axis of symmetry becomes larger due to the increase in temperature leading to the weakening of the polarization of the PMN-PT. The weak electrostatic induction of PMN-PT to the charge in the two electrodes leads to the redistribution through the external circuit to achieve a new electrostatic balance. Notely, the direction of electron migration at this point is from the upper silver electrode into the working electrode (a positive current). Therefore, it can be determined that the direction of polarization inside the PMN-PT is upward (from negative bound charge to positive bound charge). On the contrary, as the temperature of the sample decreases from 20 to 100 °C ($dT/dt < 0$), the vibrational amplitude of the electric dipole decreases, leading to an increase in the polarization intensity. The electrostatic balance is broken again, and the direction of electron migration at this point is from the working electrode into the upper silver electrode (a negative current) to reach a new stable state. Such wiring is called a forward connection. However, if a reversed connection is executed, the obtained current signals are switched in sign due to the reversal of the polarization direction of the PMN-PT with respect to the loop, as shown in Fig. S1(c) and S1(d).

Section 2 Calculation of the enhancement factor

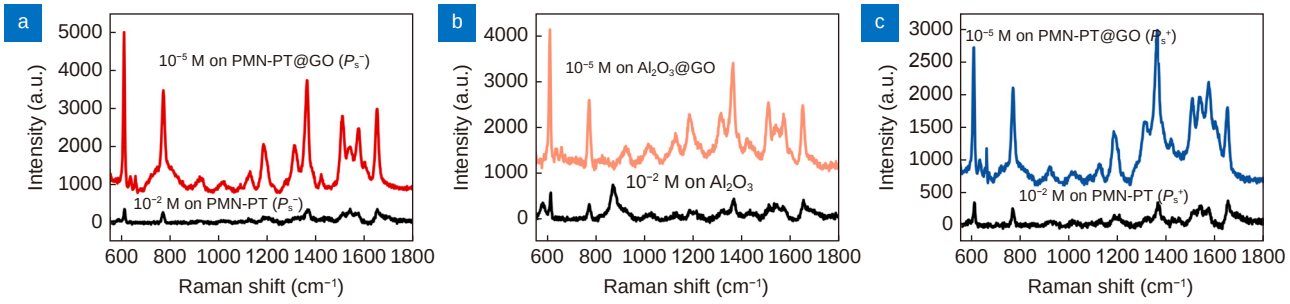

Fig. S2 | The SERS spectra of R6G (10^{-5} M) collected from PMN-PT@GO(P_s^-), Al_2O_3@GO and PMN-PT@GO (P_s^+) as well as the Raman spectra of R6G (10^{-2} M) collected from PMN-PT(P_s^-), Al_2O_3 and PMN-PT(P_s^+).

The enhancement factor (EF) was calculated using the following formula:

$$EF = \frac{I_{\mathrm{SERS}} \times N_{\mathrm{Raman}}}{I_{\mathrm{Raman}} \times N_{\mathrm{SERS}}}, \tag{S1}$$

where I_{SERS}, I_{Raman}, N_{Raman} and N_{SERS} represent the SERS signal intensity of coating GO, the Raman signal intensity of without coating GO, the number of probe molecule within laser spot on the substrate of without coating GO and the number of probe molecule within laser spot on the substrate of coating GO, respectively. The Raman spectrometer was all used under the condition (0.58 mW laser power, ×50 objective lens and 1 μm the laser spot). 5 μL R6G solution was dropped on the substrate, and the estimated diameter after drying was about 4 mm. The average areal density (AD) of R6G can be estimated by the following equation: $AD = CVN/S$, where C, V, N and S refer to the concentration of R6G, the volume of dropped R6G solution, Avogadro constant and the area of R6G molecule covered, respectively. Therefore, the EF of PMN-PT@GO(P_s^-), Al_2O_3@GO and PMN-PT@GO (P_s^+) can be obtained.

Section 3 The homogeneity of the SERS substrates

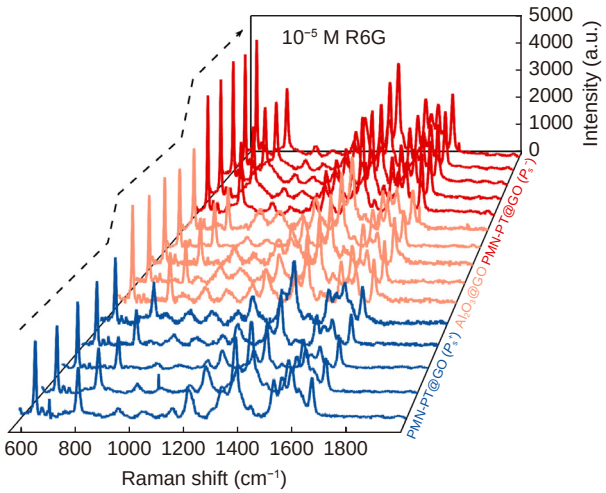

Fig. S3 | The SERS spectra of R6G collected from five random points of PMN-PT@GO(P_s^-), Al_2O_3@GO and PMN-PT@GO (P_s^+), respectively.

Section 4: Calculation of Fermi level

Under electrical contact, the contact potential difference (V_{CPD}) between the Au tip and the sample is defined as:[1]

$$V_{CPD} = \frac{\Phi_{tip} - \Phi_{sample}}{-e}, \tag{S2}$$

in which e is electronic charge, Φ_{tip} and Φ_{sample} refer to the work functions of the Au tip and the sample, respectively. And the work function Φ equal to the vacuum level E_{VAC} minus the Fermi level E_f[2].

Section 5: Herzberg-Teller coupling term *C*[3]

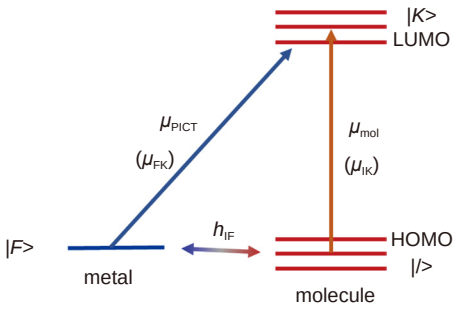

Fig. S4 | Schematic diagram of PICT process from metal-phase substrate to molecule. |*F*> is Fermi state of metal, |*I*> and |*K*> represent the ground state and the excited state of molecule, respectively, and h_{IF} refers to the Herzberg-Teller coupling term.

The simplified expression representing the electronic transition from metal-phase substrate to molecule is:

$$R_{IFK}(\omega) = \frac{\mu_{KI}\mu_{FK}h_{IF} < i|Q_k|f >}{((\varepsilon_1(\omega) + 2\varepsilon_0)^2 + \varepsilon_2^2)((\omega_{FK}^2 - \omega^2) + \gamma_{FK}^2)((\omega_{IK}^2 - \omega^2) + \gamma_{IK}^2)}, \tag{S3}$$

where ω is the frequency of the excited laser. The PICT resonance occurs at $\omega = \omega_{FK}$, and the molecular resonance occurs at $\omega = \omega_{IK}$.

Section 6: Supplementary SERS spectra of R6G under 785 nm excitation laser

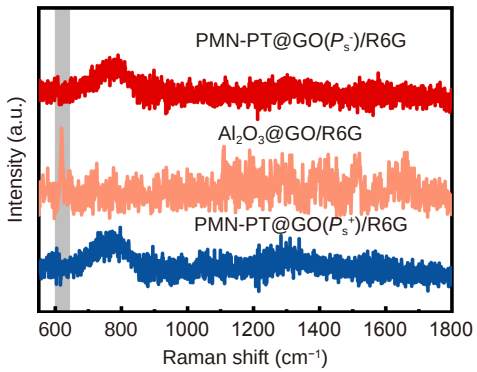

Fig. S5 | SERS performance of Al_2O_3@GO, PMN-PT@GO (P_s^+) and PMN-PT@GO(P_s^-) by employing R6G as the probe molecule under excitation of 785 nm laser.

Section 7: Supplementary SERS spectra of R6G with different concentrations on PMN-PT@GO(P_s^-)

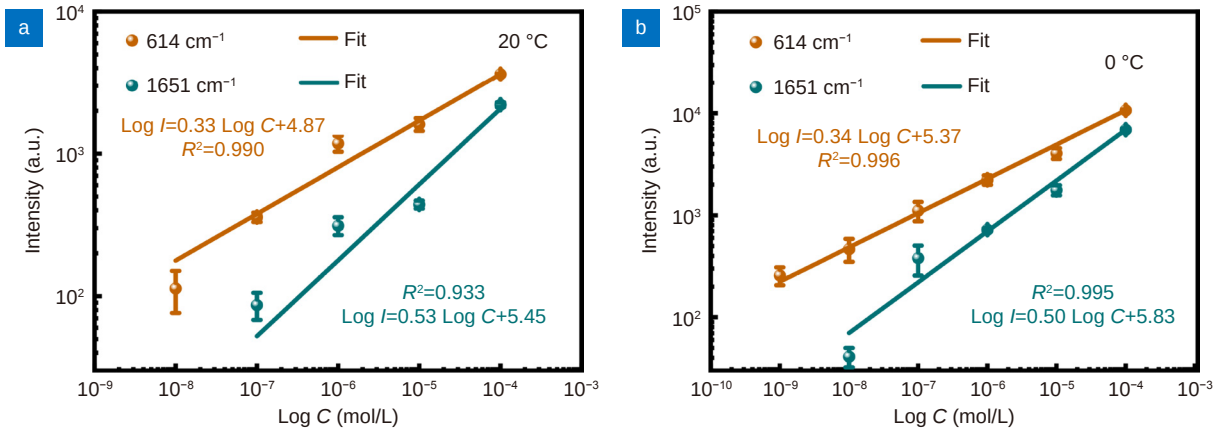

Fig. S6 | Log-log plot of average intensity of SERS signals at 614 and 1651 cm⁻¹ versus the concentrations of R6G on PMN-PT@GO (P_s^-) at (a) 20 °C, (b) 0 °C.

Section 8: Degradation experiments of substrate

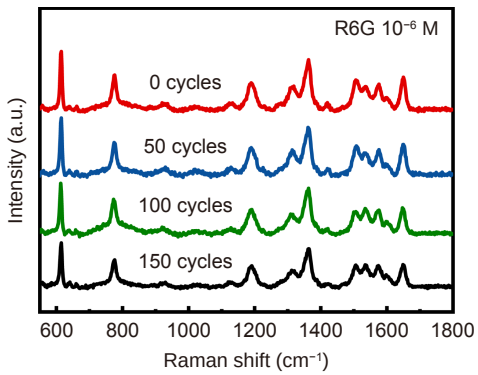

Fig. S7 | SERS spectra of R6G on PMN-PT@GO(P_s^-) substrate after different number of cycles in the temperature range of 0 to 40 °C.

Section 9: SERS spectra of R6G on PMN-PT@GO(P_S^-) with 532 or 633 nm laser

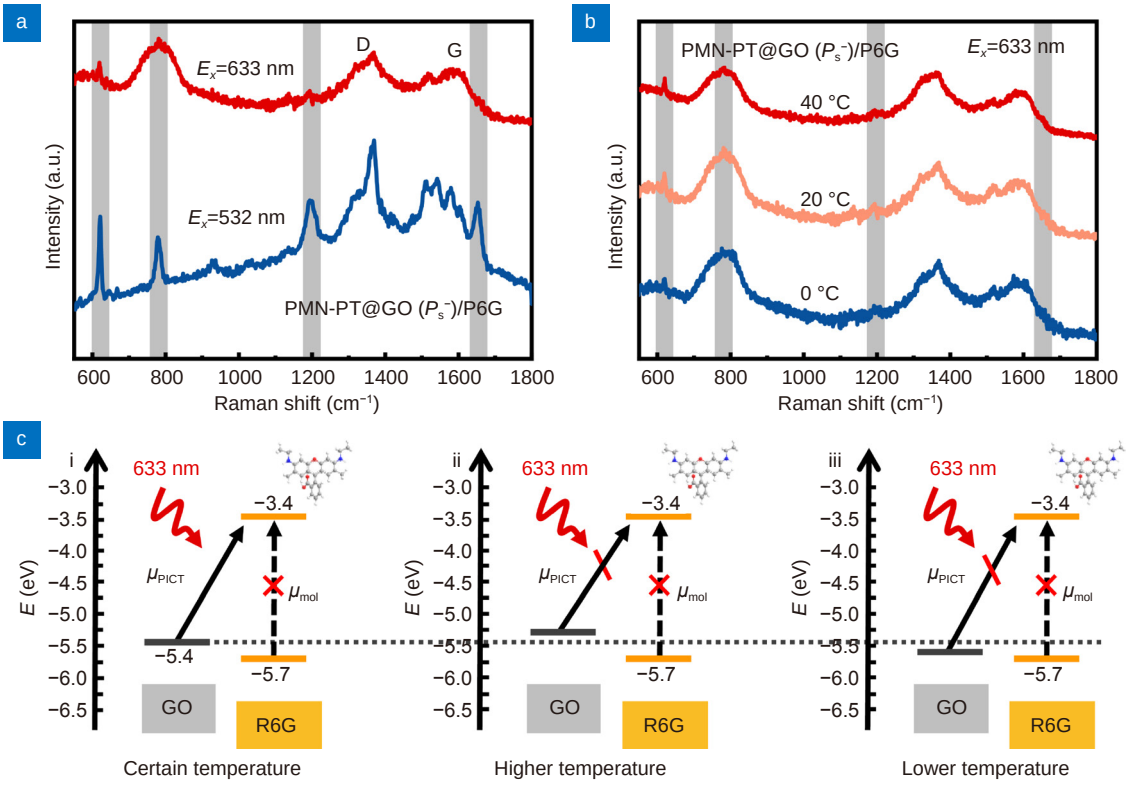

Fig. S8 | (**a**) SERS spectra of R6G on PMN-PT@GO(P_S^-) under excitation of 532 and 633 nm laser. (**b**) The temperature-dependent SERS spectra of R6G on PMN-PT@GO(P_S^-) under excitation of 633 nm laser. (**c**) Schematic illustration of the energy band structure of PMN-PT@GO(P_S^-)/R6G and the electron transition process under 633 nm excitation laser.

Section 10: Supplementary SERS spectra of CV with different concentrations on PMN-PT@GO(P_S^-)

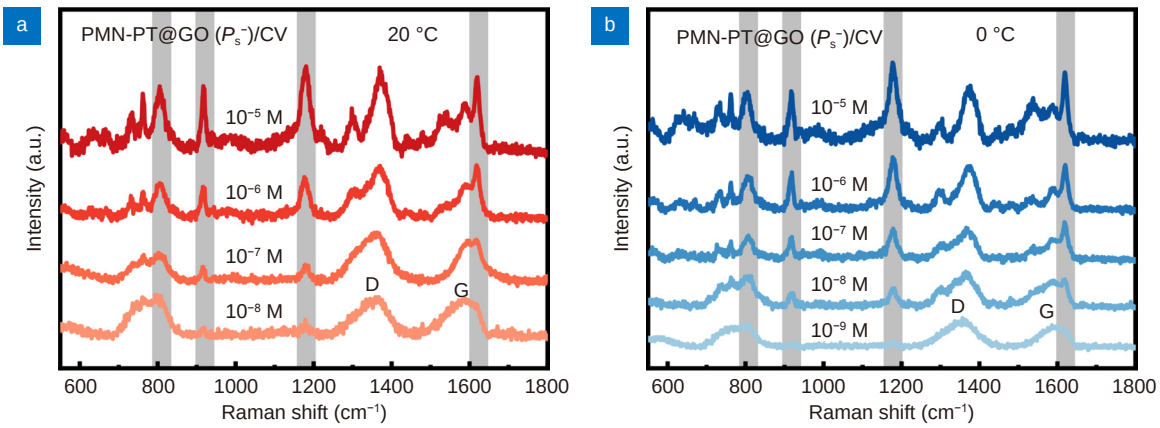

Fig. S9 | SERS spectra of CV with different concentrations on PMN-PT@GO(P_S^-) at (a) 20 °C, (b) 0 °C under 633 nm excitation laser.

Section 11: Supplementary SERS spectra of MB

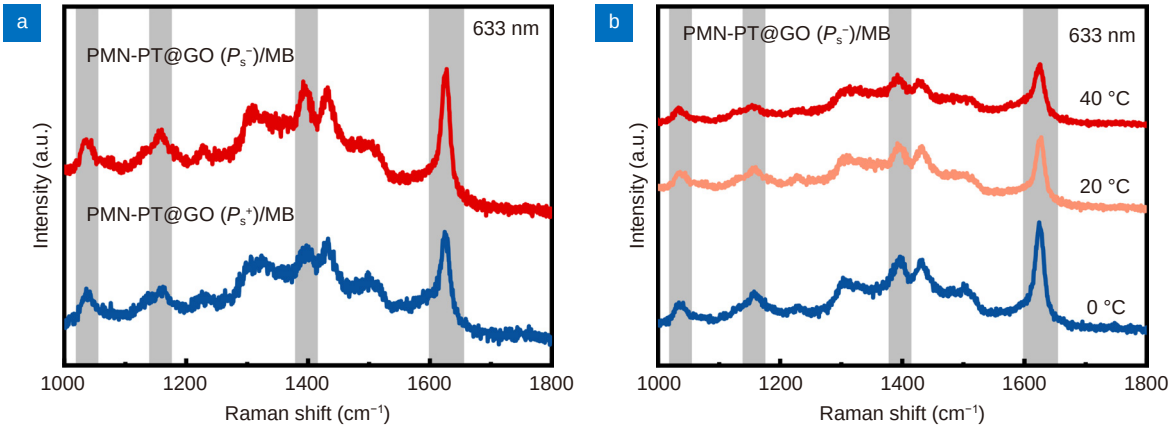

Fig. S10 | SERS performance of PMN-PT@GO (P_S^-) and PMN-PT@GO(P_S^+) by employing MB as the probe molecule under excitation of 633 nm laser.

Section 12: Selective enhancement of SERS spectra of mixed solutions

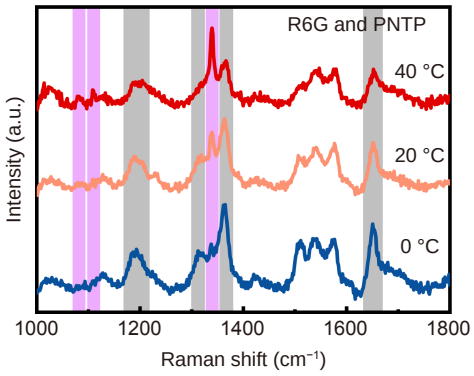

Fig. S11 | Selectively enhanced SERS spectra of mixed solutions of R6G (gray) and PNTP (violet) on PMN-PT@GO(P_S^-) substrate under 532 nm excitation laser.

Section 13: SERS spectra of PNTP on different substrates

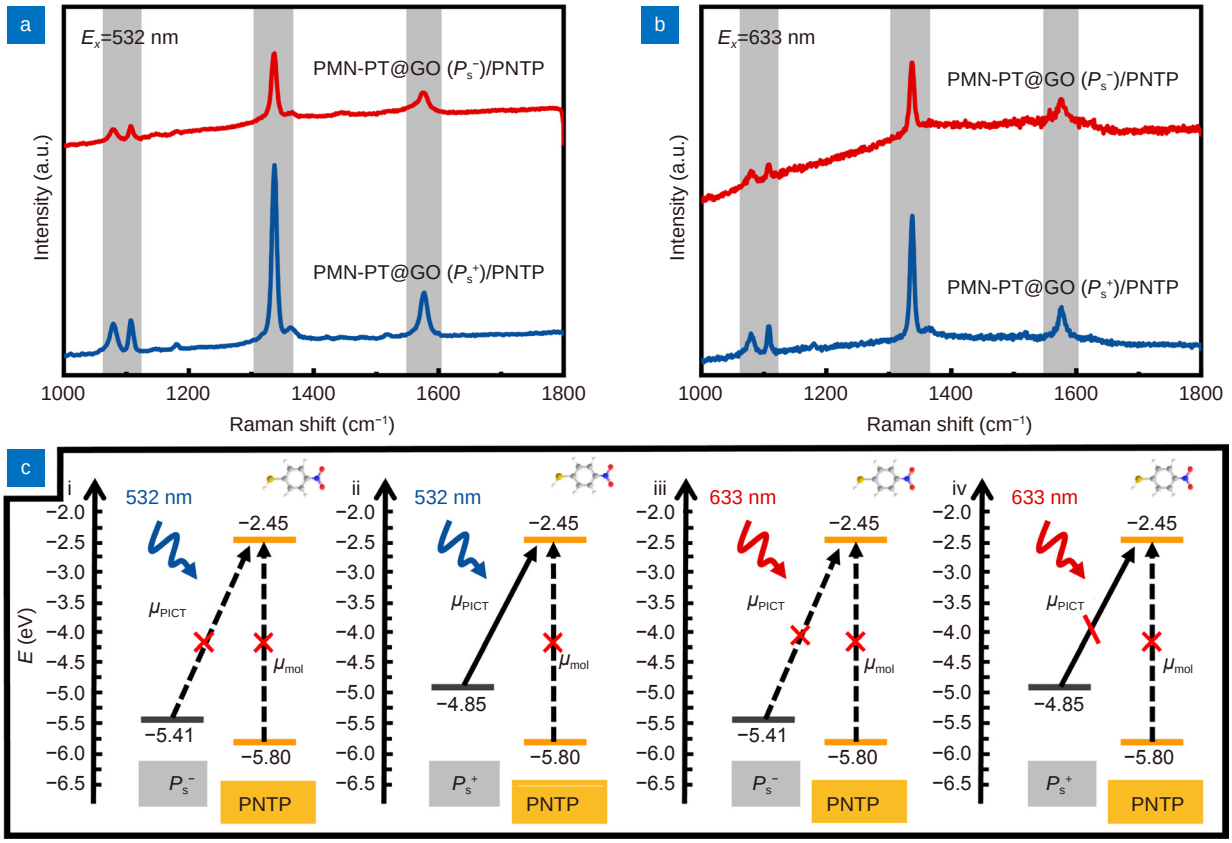

Fig. S12 | (**a**, **b**) SERS performance of PMN-PT@GO (P_s^-) and PMN-PT@GO(P_s^+) by employing PNTP as the probe molecule under excitation of (a) 532 nm, (b) 633 nm laser. (**c**) Schematic illustration of the energy band structure of (**i**, **iii**) PMN-PT@GO(P_s^-)/PNTP, (**ii**, **iv**) PMN-PT@GO(P_s^+)/PNTP and corresponding the electron transition process under 532 or 633 nm excitation laser.

Section 14: Temperature-dependent SERS spectra of PNTP on PMN-PT@GO(P_s^+)

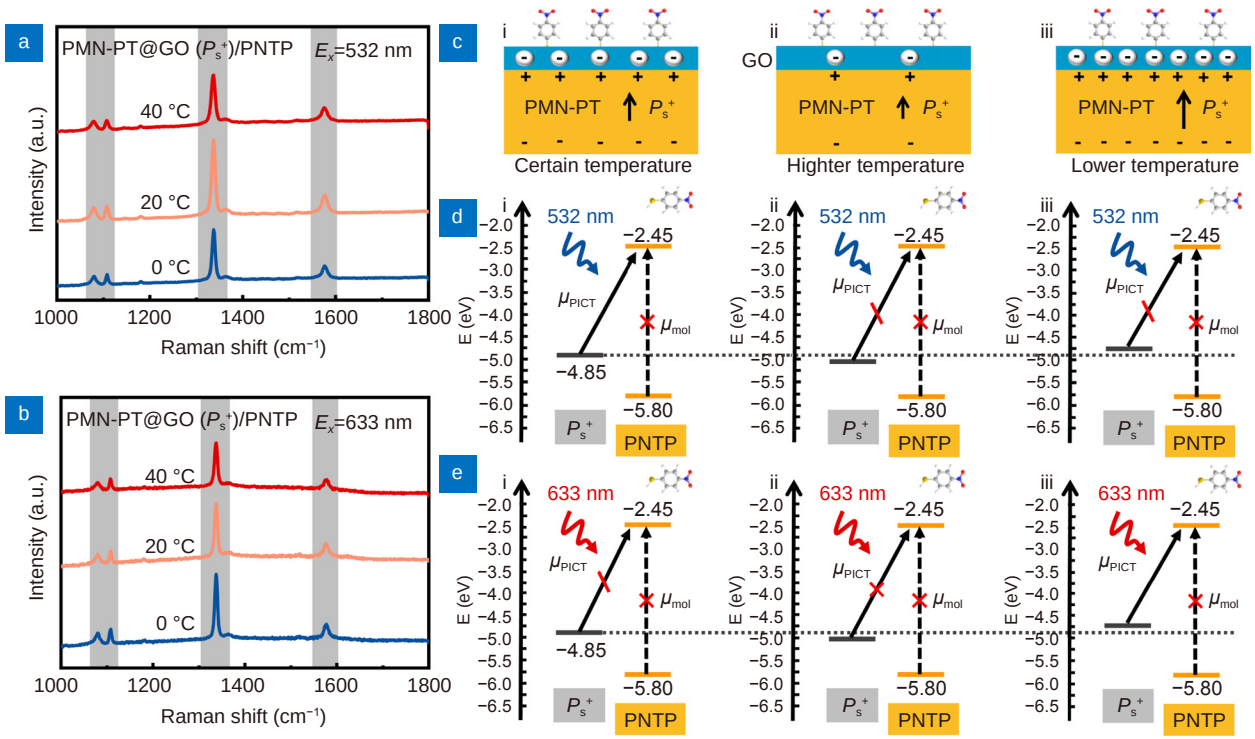

Fig. S13 | (**a**, **b**) SERS spectra of PNTP on PMN-PT@GO(P_s^+) under excitation of (a) 532 nm, (b) 633 nm laser at different temperature. (**c**) Schematic diagram of doping level of GO affected by PMN-PT@GO(P_s^+) temperature. (**d**, **e**) Schematic illustration of the energy band structure of PMN-PT@GO(P_s^+)/PNTP and the electron transition process under (d) 532 nm, (e) 633 nm excitation laser.

Section 15: Supplementary SERS spectra of PNTP with different concentrations on PMN-PT@GO(P_s^+)

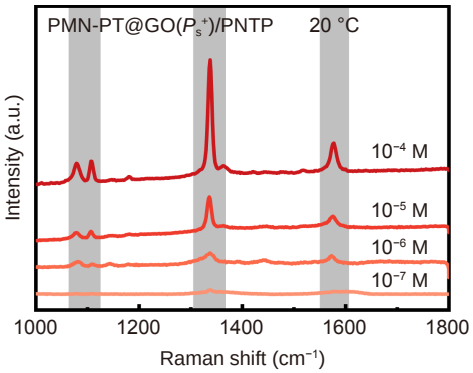

Fig. S14 | SERS spectra of PNTP with different concentrations on PMN-PT@GO(P_s^+) at 20 °C under 532 nm excitation laser.

Section 16: Experimental section

Synthesis of the substrates. The PMN-PT single crystal (<001>, 10×10×0.5 mm^3) was grown by modified Bridgman method. The Al_2O_3 crystal was purchased from Core Three Semiconductor Technology (Suzhou) Co. Graphene oxide dispersion was purchased from Pioneer Nano Technology (Jiangsu) Co. Graphene oxide dispersion (500 μL) was dropped on the substrates and subsequently the graphene oxide nanosheets were immobilized on the substrates using the spin coating method at 1500 rad/min (30 s) to prepare the Al_2O_3@GO, PMN-PT@GO (P_s^+) and PMN-PT@GO(P_s^-), respectively.

Characterization. UV-Vis-NIR spectrophotometers was used to measure absorption spectra. Kelvin probe force microscopy (KPFM) was carried out on the SmartSPM system to measure the surface potential of the sample using a gold probe as reference. A temperature control platform was employed to precisely control the temperature of the substrate

by connected software. SERS measurements were performed using the Raman spectrometer (Horiba HR Evolution) with the 50× objective lens. 5 μL of the solution of the molecule to be measured was dropped onto the sample, dried and used for spectral acquisition. The SERS spectra were obtained with 8 s acquisition time under 532 or 633 nm laser excitation.

Density functional theory calculations. The first-principles calculations were performed within the frame of the generalized gradient approximation (GGA) proposed by Perdew, Burke, and Ernzerhof (PBE) in the Vienna *ab initio* simulation package (VASP). To get the accurate structure, we adopt DFT-D2 method to optimize molecular structures. All atoms use the pseudopotentials recommended by VASP. The cut off energy was chosen to 550 eV. The convergence criterion of energy in relaxation was set to be 10^{-5} eV. The Γ centered k-grids were adopted 6×4×1 for all slabs. For geometry optimization, we fully relax the bulk systems until the Hellmann-Feynman forces were less than 0.05 eV/Å. After the optimization of bulk systems, the <001> surface was cleaved, followed by the construction of more than 25 Å vacuum layer added to the unit cell of the layers to simulate periodic boundary conditions. Then, we constructed two models, one is the adsorption of Pb-O surface and graphene layer (2×5×1), and the other is the adsorption of B-O surface and graphene layer.

References

S1. Ma ZM. *The Kelvin Probe Force Microscopy and its Related Technology with High Sensitivity and High Resolution* (Tsinghua University Press, Beijing, 2019).

S2. Kahn A. Fermi level, work function and vacuum level. *Mater Horiz* **3**, 7–10 (2016).

S3. Lombardi JR, Birke RL. A unified approach to surface-enhanced Raman spectroscopy. *J Phys Chem C* **112**, 5605–5617 (2008).